Materials Science & Engineering A 810 (2021) 140979

Contents lists available at ScienceDirect

Materials Science & Engineering A

journal homepage: http://www.elsevier.com/locate/msea

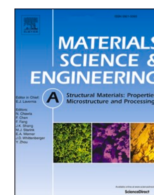

Achieving high-strength metallurgical bonding between A356 aluminum and copper through compound casting

Aina Opsal Bakke, Lars Arnberg, Yanjun Li *

Norwegian University of Science and Technology, Alfred Getz' Vei 2, 7034, Trondheim, Norway

ARTICLE INFO

Keywords:
Compound casting
Aluminum A356
Intermetallics
Sessile drop test
Tensile test

ABSTRACT

Due to stable surface oxides on the solid copper surface and the ease of forming Al_2O_3 films at the aluminum melt surface, it is difficult to achieve high-strength metallurgical bonding between the two materials through compound casting. In this research, a novel surface coating method for the copper inserts, namely hot-dip Sn-coating, has been applied. Through this method, a high-quality bond between a cast aluminum alloy A356 and commercially pure copper was achieved through a gravity compound casting process. Tensile tests showed that a maximum ultimate tensile strength (UTS) of 90.8 MPa could be obtained for the bimetal interface. Microstructures formed in the aluminum/copper interface were studied by optical- and scanning electron microscopy, while a sessile drop wetting test was used to study the wettability between the aluminum melt and Sn-coated copper substrates. The effects of Sn-coating on the wettability and the formation of interfacial microstructure were discussed.

1. Introduction

Bimetallic Al/Cu components can combine the high thermal and electrical conductivity of copper and the lightweight and good corrosion properties of aluminum. Such components are therefore used in bus bars, yoke coils and armored cables, to name a few applications [1–4]. It has been suggested that as much as a 40% weight reduction and 60% cost reduction can be achieved in using Al/Cu bimetals compared to Al–Cu alloys [1].

Various methods have been used to create Al/Cu bimetallic components, such as friction welding [5], friction stir welding [6], cold rolling [7], rod extrusion [8] and ultrasonic welding [9]. As Cu and Al have a high affinity towards each other, especially at temperatures exceeding 120°C, brittle intermetallic phases can easily form when joining the two materials [10,11]. This reduces the overall bonding strength of the component. Wang et al. showed an almost linear decrease in tensile strength with increasing thickness of the intermetallic phases [12]. The tensile strength of flash welded Al//Cu components decreased from approximately 57 MPa at 5 μm thickness of intermetallic layers to approximately 6 MPa at 60 μm, while brazed Al//Cu components showed a decrease from approximately 60 MPa at 3 μm to 22 MPa at 47 μm. Pan et al. reported a tensile strength of 88 MPa in the center of a friction welded Al//Cu joint where the intermetallic layer was 0.8 μm thick [13], while Asemabadi, Sedighi and Honarpisheh measured a tensile strength of 227 MPa in an explosively welded Al//Cu joint where no intermetallic phases were detected [14]. As a low temperature solid-state joining process, friction stir welding (FSW) appears to be an effective method to prevent formation of thick intermetallic layers in the interface [15]. Thus, high-strength bonding between the two materials can be achieved, with tensile strength ranging from 105.8 MPa to 200 MPa being reported [6,16,17]. However, most welding processes are limited to applications on plate-shaped work pieces. Compared to the mentioned welding methods, compound casting is a simpler joining process with less geometrical restrictions. In the process, two materials, one in solid state and the other liquid, are joined together by the liquid material being cast around the solid. When the two materials come in contact, a diffusion zone will form between them, forming a layer of intermetallic phases and thus a metallurgical bond [18,19]. Recently, a similar process, named composite casting, has been applied to join aluminum and copper. In this process, copper is first cast into the mold and then as the copper solidifies, aluminum is cast onto it [20].

During the compound casting process, a good wettability between the liquid aluminum and solid copper is crucial in achieving a strong bond. On both aluminum and copper, stable surface oxides lead to significant reduction in wettability. Various approaches have been tried to remove the oxide layer and thus ensure good bonding. Jiang et al. joined

* Corresponding author.
E-mail address: yanjun.li@ntnu.no (Y. Li).

https://doi.org/10.1016/j.msea.2021.140979
Received 22 October 2020; Received in revised form 21 January 2021; Accepted 16 February 2021
Available online 24 February 2021
0921-5093/© 2021 The Author(s). Published by Elsevier B.V. This is an open access article under the CC BY license (http://creativecommons.org/licenses/by/4.0/).

aluminum A356 and copper through a lost foam compound casting (LFC) process, where the gas formed when decomposing the foam pattern could protect the metals from oxidation [21]. Using this process, a continuous bonding was achieved. However, thickness of the eutectic Al–Al_2Cu reaction layer exceeded 1.5 mm in certain areas, which is expected to be detrimental to the strength. As a result, a bonding strength as low as approximately 28.5 MPa was measured. Another method of increasing wettability between the two metals, is to use a coating layer. Zn, which has a melting point of 420°C [22], has shown promising results for joining Al/Mg [23] and Al/Steel [24]. During compound casting, the melting of the Zn-layer will leave an oxide-free surface, which improves the wettability of the solid metal to the liquid metal and enhances the formation of a metallurgical bond. The effect of thermal spray Zn-coating onto Cu inserts in a squeeze casting with aluminum was investigated by Liu et al. [3]. They found that the Zn-layer enhanced wettability and caused formation of a metallurgical bond. A maximum UTS of 26 MPa was achieved for the compound casting, where the fracture was found to propagate through the Al_2Cu intermetallic layer and the eutectic Al–Al_2Cu layer. However, Zn was found to aggregate at the interface in the compound casting when a pouring temperature of 680°C was used, showing that Zn is not an optimal coating layer for low casting temperatures.

Mechanical properties of Al/Cu bimetals can also be improved by using Ni-coating. Zhao et al. found that by using Ni-plated aluminum for Al/Cu diffusion bonding, the tensile shear strength could be increased from 14.3 MPa to 25.9 MPa. This was due to the formation of Al–Ni intermetallic phases at the interface, which have lower growth rate than Al–Cu phases and thus cause a thinner reaction layer [25]. Hu et al. studied the effect of electroless plated Ni–P coating of pure Cu sheets on Al/Cu compound castings. Results showed that thickness of the reaction layer was reduced while the metallurgical bonding was improved. It was suggested that the P in the coating layer reacts with copper oxide, which will enhance the wettability, and that the Ni layer can hinder Al diffusion into the Cu sheet, thus reducing growth of intermetallic phases [19]. In a previous work by the authors [26], only local areas of metallurgical bonding between Cu and aluminum A356 could be achieved through an industrial scale low pressure die casting process without the use of surface treatment. The typical interfacial microstructure in the bonded region consisted of primary Si particles among the coarse eutectic Al–Al_2Cu phase. The formation of primary Si particles was attributed to phosphorous present in the Cu as a common impurity element, which forms AlP in the liquid aluminum in the reacted region, acting as heterogeneous nucleation sites for primary Si.

In this research, an innovative hot-dip Sn-coating process has been used on solid Cu to increase wettability. The effect of Sn-coating on the wetting behavior between the liquid A356 aluminum alloy and Cu substrate, and the solidification structure formed at the interfaces of both wetting test samples and compound castings have been systematically investigated. Strength of the interfacial bonding of the compound castings has been measured by tensile testing.

2. Materials and methods

2.1. Casting experiment

Commercially pure copper pipes, made from phosphorus-deoxidized copper (0.015–0.040 wt% P), of 10 mm in diameter, 1 mm in thickness and 100 mm in length were used as solid inserts for compound castings. To make compound castings for tensile testing, copper plates with dimensions of 0.7 mm × 50 mm × 50 mm were also used as inserts. For comparison, some of the pipes were ground with 1200 grit paper and cleaned thoroughly in 96% ethanol with no further coating treatment. The remaining copper pipes and copper plates were coated with a Sn-layer. These inserts were ground with 1200 grit paper, cleaned in ethanol, then immersed into a 10% NH_4Cl solution for 5 min at 75°C and air-dried. Commercially pure Sn was melted to 400°C in an induction furnace. The inserts were preheated to 100°C, before being immersed into the Sn-bath for 2 min. Prior to casting, the Sn-coated inserts were slightly ground with 1200 grit paper and cleaned in ethanol. The pipes were then placed in a graphite mold, shown in Fig. 1a. The mold with the copper pipe were placed in an induction furnace and preheated to 200°C. Copper plates were placed in a copper mold, shown in Fig. 1b, with mold cavity diameter and height designated as d_i and h_i, and total mold diameter and height as d_o and h_o respectively. Neither the copper plates nor copper mold were preheated prior to casting.

A commercial cast aluminum alloy A356 was melted in an induction furnace at 800°C. A ladle was used to pour liquid A356 into the molds, with a pouring temperature of 730°C. Chemical compositions of the alloy are given in Table 1.

2.2. Wetting tests

Commercially pure copper cylinders with 10 mm diameter and 3 mm thickness were Sn-coated in a similar process as the casting inserts. Small pieces of A356 were cut to a weight of 0.0300 g ± 0.0011 g. Both coated and uncoated copper samples were slightly ground with 800 grit paper prior to the wetting test. All copper samples and A356 pieces were cleaned in a beaker with acetone immersed into an ultrasonic bath for 5 min.

After drying, an A356 sample piece together with a copper substrate were put in a graphite sample holder and then inserted into the heating chamber in the wetting furnace. Pressure inside the chamber was lowered to approximately 10^{-5} mbar before the heating elements were turned on. The sample was heated to 750°C through a two-step process: First from room temperature to 600°C with a heating rate of 4°C/s, then from 600°C to 750°C at 2.5°C/s. A normal casting temperature of A356 alloy, 750°C, was chosen to simulate a real casting process. The evolution of the A356 solid piece and later droplet was recorded by a camera, with a frequency of one picture per second, during the wetting experiment.

2.3. Tensile testing

Tensile test samples with a thickness of 1 mm and a gauge length of 6 mm were cut from the compound castings with copper plates in the middle of the gauge. Dimensions of the tensile samples are shown in Fig. 2, with the copper plate indicated by the shaded area. Tensile tests were conducted using a Zwick/Roell Z2.5 machine with a 2.5 kN load cell and a video extensometer. Strain rate was set to $5 \cdot 10^{-4}$ s^{-1}. Ultimate tensile strength (UTS) of the castings was determined from the tensile tests.

2.4. Microstructure characterization

To characterize the interfacial structure in the Al/Cu castings, cross-sections of the compound castings were cut perpendicular to the casting direction, whereas the solidified wetting test samples were first mounted in epoxy then cut in half to get a cross section of the interface between the Al droplet and Cu substrate. All samples were then ground up to 4000 grits on a Struers LaboPol-21, followed by polishing with 3 μm and 1 μm polishing suspension on a Struers Tegramin-20. The cast samples were in addition polished with a Buehler Vibramet 2 for at least 10 h. Microstructure characterization was conducted using a Zeiss Supra 55VP Low Vacuum Field Emission Scanning Electron Microscope (LVFESEM) and a Zeiss Ultra 55 Field Emission Scanning Electron Microscope (FESEM). The intermetallic phases formed in the interface were analyzed using Energy Dispersive Spectroscopy (EDS), Electron Backscatter Diffraction (EBSD) and a JEOL JXA-8500F Electron Probe Micro Analyzer (EPMA).

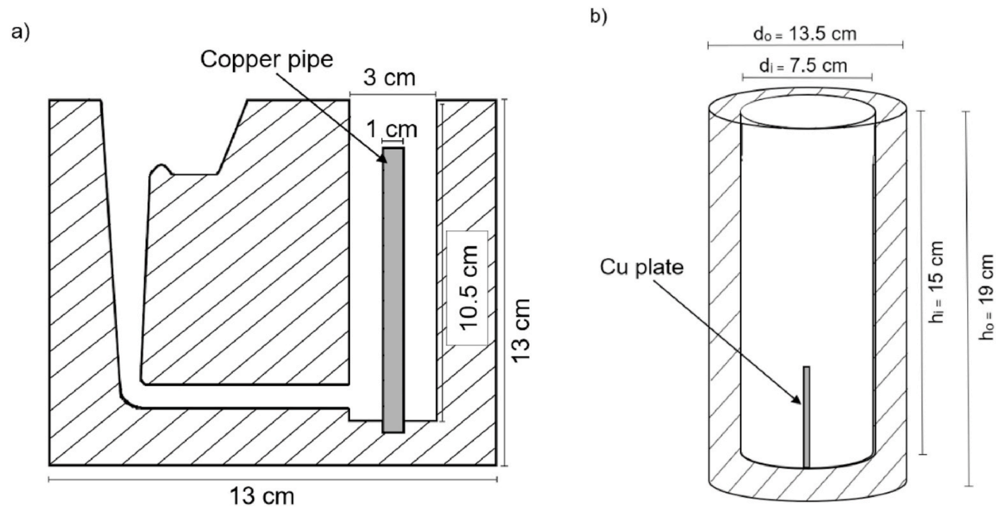

Fig. 1. Sketch and dimensions of the casting molds. a) Graphite mold with copper pipe inserts, b) Copper mold with copper plate inserts.

Table 1
Chemical composition of the A356 aluminum alloy.

Alloy	Composition [wt.%]								
	Si	Mg	Ti	Fe	Sr	Ga	Zn	Others	Al
A356	7.0	0.41	0.11	0.082	0.013	0.0089	0.0042	0.0029	Bal.

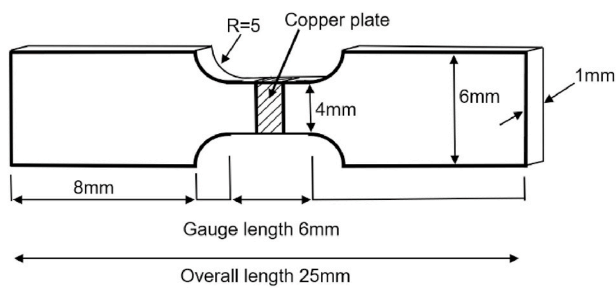

Fig. 2. Dimensions of the tensile samples. The copper plate was placed in the middle of the sample as indicated by the shaded area.

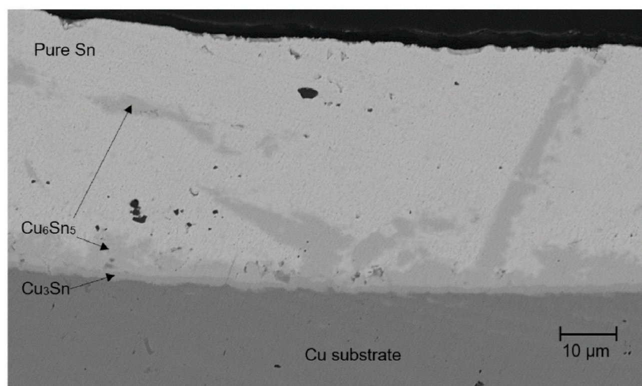

Fig. 3. BSE image of the Sn-coating layer on the Cu substrate prior to the wetting experiment.

3. Results

3.1. *Influence of Sn-coating on wetting behavior*

Fig. 3 shows a backscattered electron (BSE) image of the Sn coating layer on the copper substrate prior to the wetting experiment. It can be seen that the coating layer shows good bonding with the copper substrate. From the contrast variations, two intermetallic phases in addition to the copper substrate and bright pure Sn have formed in the coating layer. At the interface between Sn and copper, the thin layer of intermetallic phase was detected to have a composition of approximately 75 at.% Cu and 25 at.% Sn by EDS, whereas the larger phase observed both at the Cu/Sn interface and in the Sn-layer showed compositions of around 56 at.% Cu and 44 at.% Sn. These compositions coincide with Cu_3Sn and Cu_6Sn_5 respectively. The thickness of the coating layer is approximately 40 μm.

Fig. 4 shows the evolution of the A356 sample on top of an uncoated Cu substrate as a function of holding time during heating at 750°C.

After heating to 750°C, a slight rounding of the corners of the A356 sample can be seen in Fig. 4a. After 2 min heating at 750°C, the A356 piece changed into a more round shape (Fig. 4b), showing that the solid A356 sample has partially melted. Fig. 4c, shows the image of the A356 sample after holding at 750°C for 9 min. All corners of the original solid sample have become round, indicating a complete melting of the A356 sample. However, it does not show a typical spherical droplet shape. This is believed to be a result of the thick oxide layer on the surface of the A356 sample, which constrains the free-shape evolution of the droplet. At the bottom of the A356 droplet, a small amount of the Al melt has flowed out (bottom left side of the droplet), spreading on the surface of the Cu substrate. It appears that a good wetting, represented by a low contact angle, exists between this part of the Al melt and the substrate. However, at the right side of the droplet bottom, a high contact angle between the droplet and the substrate can be observed, showing that the wetting test temperature used is not sufficient to break the aluminum oxide layer and cause a complete wetting between the Al melt and the Cu substrate.

Fig. 5 shows the evolution of the A356 sample on top of a Sn-coated

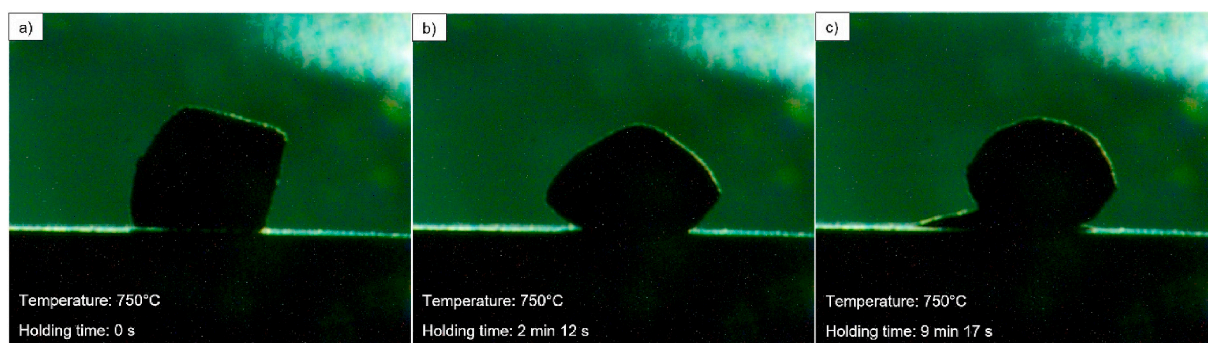

Fig. 4. Evolution of the A356 sample on top of an uncoated Cu substrate during the wetting experiment when holding at 750°C.

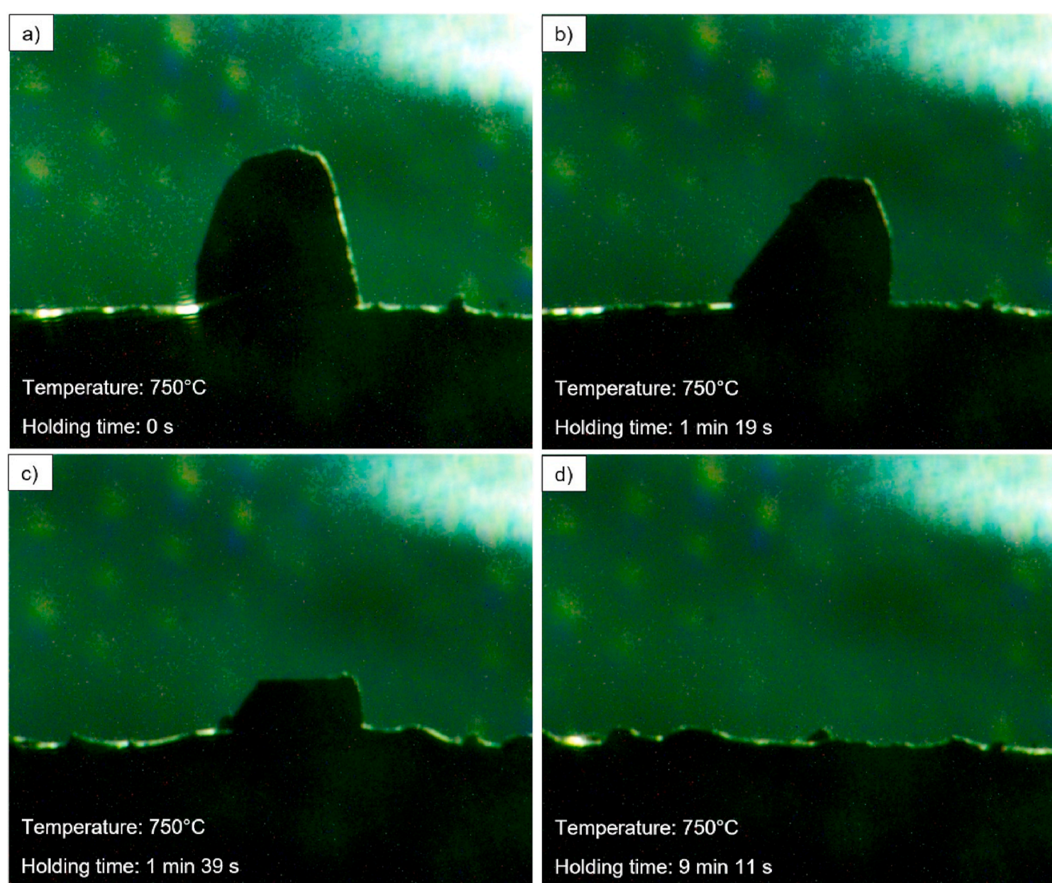

Fig. 5. Evolution of the A356 sample on top of a Sn-coated Cu substrate during the wetting experiment, when holding at 750°C.

Cu substrate during the wetting experiment.

During heating, the Sn coating layer on the Cu substrate has re-melted. As shown in Fig. 5a, after heating to 750°C, the round corners of the A356 sample indicates that partial melting has already occurred. After holding at 750°C for 1 min (Fig. 5b), a significant reduction of the height and volume of the A356 sample can be observed, implying that part of the A356 droplet has mixed with the molten Sn-layer. 20 s later, the majority of the A356 piece has spread onto the substrate (Fig. 5c). Leaving the sample at 750°C for an additional 8 min resulted in a complete disappearing of the A356 droplet, seen in Fig. 5d. This shows that a complete wetting could be achieved between the Sn-coated Cu substrate and the A356 droplet.

Fig. 6 shows optical micrographs for the as-solidified A356 droplets on the Cu substrates without and with Sn-coating. For the sample without Sn-coating (Fig. 6a), it can be seen that a reaction layer has formed between the A356 and Cu substrate, which can explain the local good wetting between the A356 droplet and the substrate shown in Fig. 4c. At the Al/Cu interface, multiple Al–Cu phases have formed, as detected through EDS. Although a metallurgical bonding was achieved, a crack can be seen propagating through the interface in the sample. This crack has likely formed upon solidification, due to different thermal expansion coefficients in the various phases. For the A356 droplet solidified on the Sn-coated Cu substrate, the surface of the substrate is completely flat after solidification, as seen in Fig. 6b. Through EDS analysis it was determined that at the surface, layers of copper-rich Al–Cu phases have formed. The layer between the surface layer and Cu substrate, observed as a yellow layer in the figure, had a consistent composition of approximately 25 at.% Al-75 at.% Cu. A similar layer can also be found in Fig. 6a, but with a much smaller thickness. High concentrations of Sn were only detected on the right corner of the Sn-coated

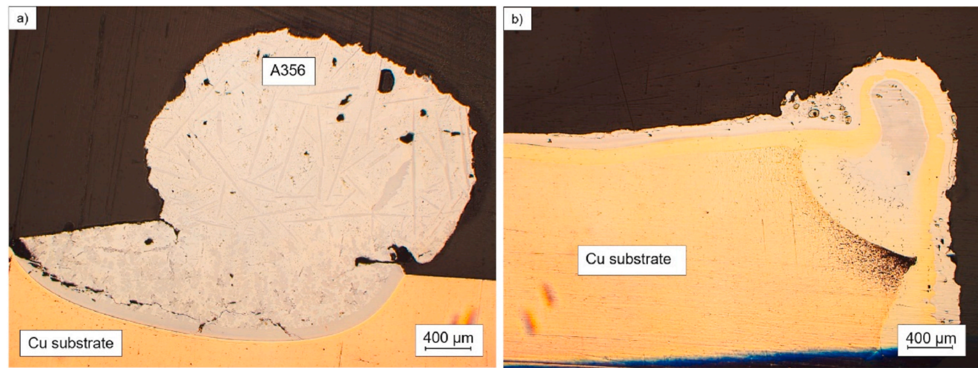

Fig. 6. Optical micrographs from the wetting experiments showing the A356/Cu interface after 10 min at 750°C. a) A356 on Cu substrate. b) A356 on Sn-coated Cu substrate.

substrate between the Al–Cu layers and the Cu substrate, where a rise of the surface layer level can be observed. When the A356 piece was completely spreading on the substrate surface, some of the liquid Sn-coating will be pushed towards the substrate edge. This was confirmed through EDS measurements of the right corner in Fig. 6b, which revealed that the substrate surface contains Cu and Al with 6–18 at.% Sn in this area, suggesting formation of bronze.

3.2. *Interface structure formation during compound casting*

Fig. 7 shows optical micrographs of the interfaces in the A356/Cu compound castings without and with Sn-coating, in Fig. 7a and b respectively. Without Sn-coating, it can be seen that no continuous bond or reaction layer exists between the A356 aluminum and Cu insert. Only small local reaction areas can be observed. Additionally, cracks can be seen in the interface. With Sn-coating, a continuous reaction layer of approximately 1 mm thickness was achieved throughout the interface, showing that Sn can significantly promote the metallurgical bonding between the A356 melt and the Cu insert.

Fig. 8 shows optical microscopy and backscattered electron (BSE) images of the microstructure of a local reaction area formed at the interface of the A356/Cu compound casting without Sn-coating. From the BSE image in Fig. 8b, the contrast difference reveals that multiple intermetallic phases have formed in the reaction area, whereas the large dark particles observed in the optical micrograph in Fig. 8a cannot be distinguished through contrast. It can be seen that cracks have formed in the reaction area during solidification, propagating through the large dark particles. Fig. 8c shows a higher magnification BSE image of the reaction layer at the Cu surface. Based on contrast, it can be seen that two intermetallic layers formed in the interface. Compositions of the observed intermetallic phases were analyzed through EDS, as shown in Table 2. Fig. 8a and b show the same area and are therefore marked with the same numbers.

From the compositions in Table 2, it can be seen that the majority of the intermetallic particles in the reaction area are the binary Al_2Cu phase (areas 1 and 4). In Fig. 8b it can be observed that the Al_2Cu phase forms both as elongated coarse particles growing from the Cu surface into the reaction area, and as a finer eutectic Al_2Cu structure within the reaction area. The large dark particles observed adjacent to the crack in Fig. 8a are determined to be primary Si particles. Smaller primary Si particles can also be observed between the eutectic structure throughout the reaction area. A phase with slightly darker contrast than the Al_2Cu phase (area 3), with a high concentration of magnesium has been determined to be Q-phase ($Al_5Cu_2Mg_8Si_6$). Between the coarse Al_2Cu phase and Cu insert, a layer of copper-rich intermetallic phases has formed (area 5 and 6 in Fig. 8c). Area 5 has been determined to be the binary AlCu phase. In area 6, a phase containing more Cu with a composition lying between those of Al_2Cu_3 or Al_4Cu_9 can be seen. It is likely that Al_4Cu_9 has formed as it is known to be the first of the copper-rich phases to form [21].

Fig. 9a shows a BSE image of the interface structure forming in the compound casting between the A356 alloy and the Sn-coated copper. As can be seen, the interface structure is quite similar to the reaction layer shown in Fig. 8. The major difference is that the reaction layer is much thicker than that without Sn-coating. Also, there are some bright particles distributed between the Al–Al_2Cu eutectic structure. It should also be noted that the Al_2Cu grains at the copper surface are larger and coarser compared to those in the fine Al–Al_2Cu eutectic structure. The chemical compositions of various phases formed in the reaction layer were determined through EDS analyses and the results are given in Table 3.

The compositions in Table 3 confirms that similar intermetallic phases have formed in the reaction layer between A356 and Sn-coated Cu. However, some differences should be noted. The particles with

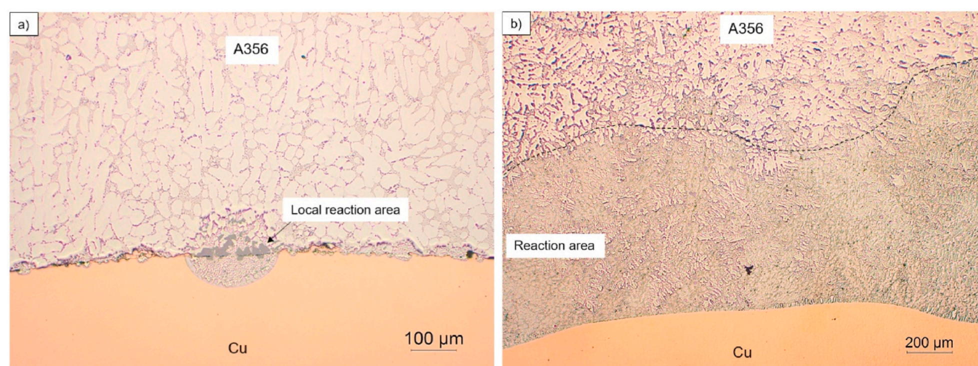

Fig. 7. Optical micrographs of the A356 aluminum/Cu interface and reaction area thickness in castings a) A356/Cu, b) A356/Sn-coated Cu.

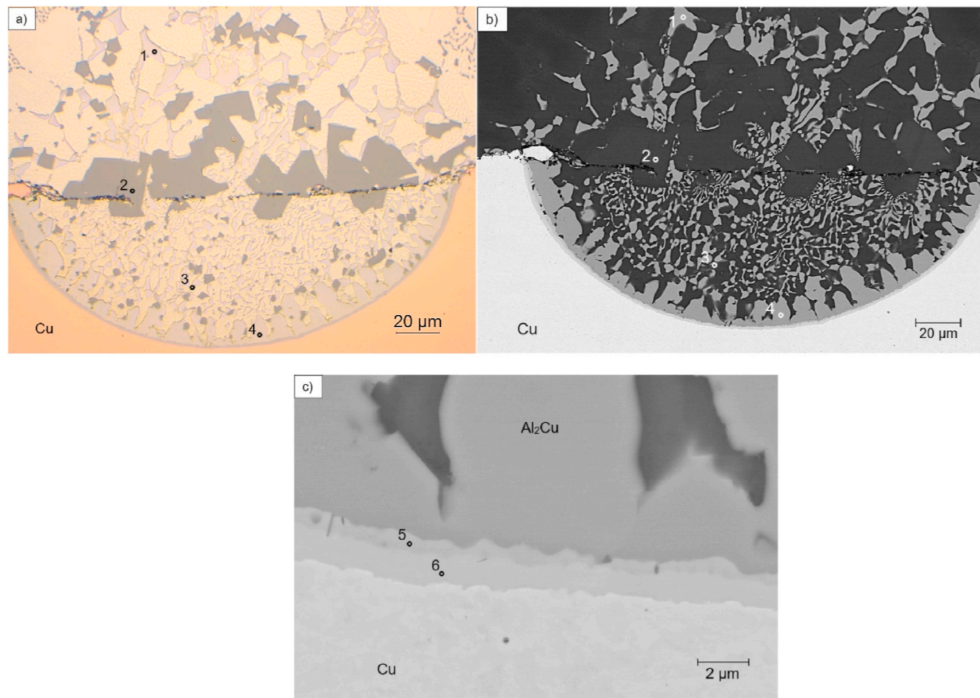

Fig. 8. One of the reaction areas formed in the A356/Cu interface in the uncoated compound casting a) Optical micrograph of a magnified local reaction region and the corresponding BSE image, b), c) Higher magnification BSE of the reaction layer at the Cu surface.

Table 2
Chemical compositions of the phases formed in a reaction area in the A356/Cu castings. Compositions were determined through EDS analyses from the areas noted in Fig. 8.

Area	Composition [at%]					Possible phase
	Al	Cu	Si	Mg	O	
1	67.06	28.32	1.09	–	3.53	Al_2Cu
2	1.52	–	98.48	–	–	Si
3	38.79	8.84	23.79	28.58	–	$Al_5Cu_2Mg_8Si_6$
4	65.54	28.04	6.42	–	–	Al_2Cu
5	47.47	51.69	0.85	–	–	AlCu
6	32.57	61.56	–	–	5.87	Al_4Cu_9

bright contrast, marked with 1 and 2 in Fig. 9a are detected to be enriched with Sn and contains some O and Mg, respectively. Since no Sn-rich phase can be seen at the interface, it suggests that the Sn-layer has melted completely during casting, forming Sn-rich particles in the Al_2Cu–Al region. Between the Al_2Cu phase and the Al_4Cu_9 phase (area 6), the composition suggests formation of a layer of Al_2Cu_3 (area 5) on the Al_4Cu_9 layer. It should also be noted that no large primary silicon particles were detected in the reaction area shown in Fig. 9a, which differs from the uncoated castings.

Fig. 10 shows the element mapping of the interface in the A356/Cu compound casting aided with Sn-coating. By comparing the distribution for Al and Si, it can be seen that there are areas where only Si is detected, suggesting that primary silicon particles also have formed in the reaction area of these castings. However, the particles detected here are

Table 3
Chemical compositions of the phases formed in a reaction area in the A356/Cu Sn-coated castings. Compositions were determined through EDS analysis from the areas noted in Fig. 9.

Area	Composition [at%]						Possible phase
	Al	Cu	Sn	Si	Mg	O	
1	45.24	3.16	35.97	–	–	15.62	Sn-rich particle
2	29.87	6.03	55.57	–	8.53	–	Sn-rich particle
3	72.87	25.07	–	2.06	–	–	Al_2Cu
4	68.91	30.14	–	0.95	–	–	Al_2Cu
5	40.07	59.93	–	–	–	–	Al_2Cu_3
6	21.58	78.42	–	–	–	–	Al_4Cu_9

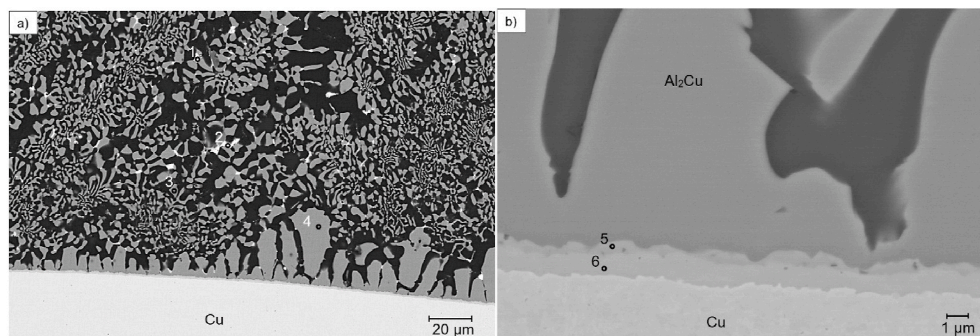

Fig. 9. BSE images of the A356/Cu interface in a casting with Sn-coating. a) Microstructure in the reaction area. b) Magnified image of the reaction layer at the Cu surface.

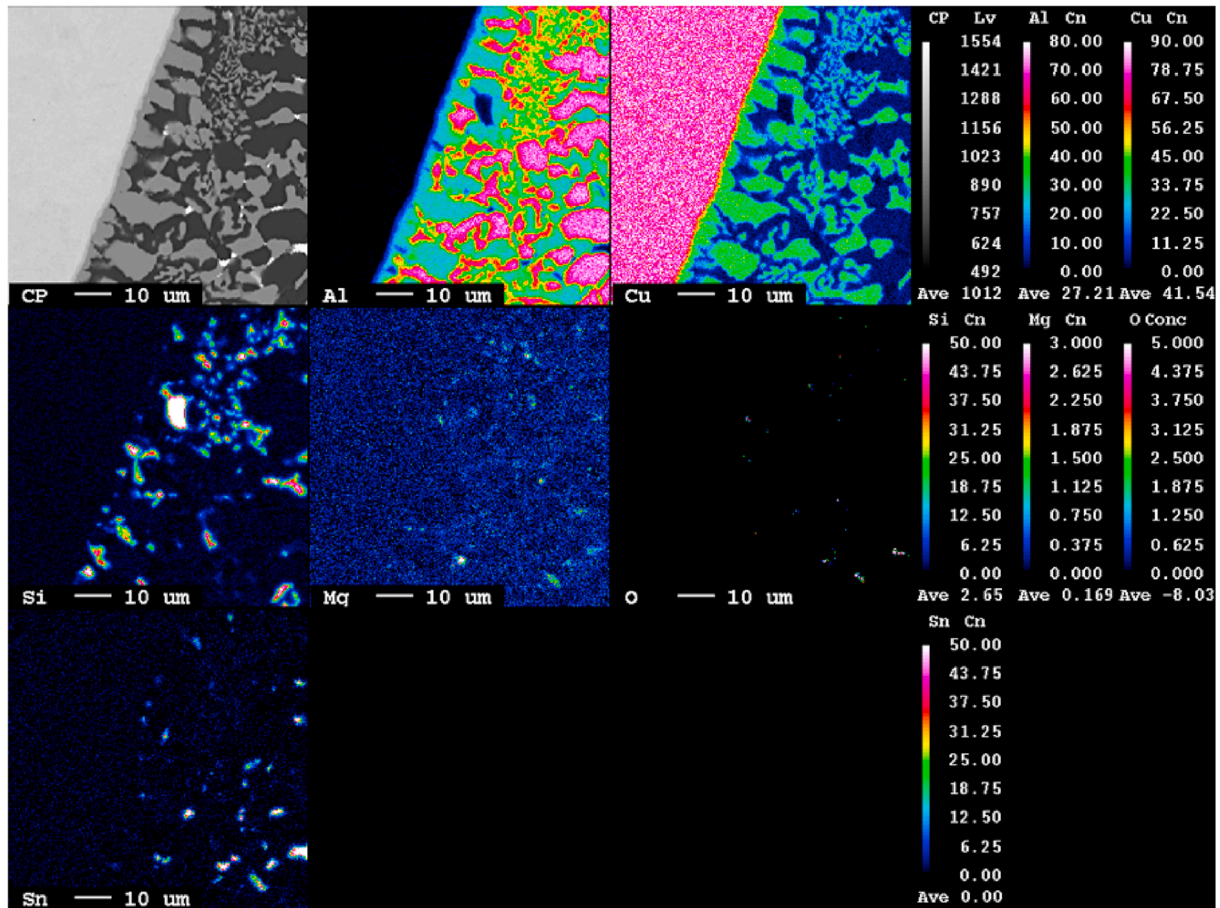

Fig. 10. EPMA map of the element distribution in the A356/Cu interface in a casting with Sn-coating.

significantly smaller than those observed in the uncoated castings in Fig. 8. The distribution of Sn confirms that no Sn coating layer remains at the Cu surface after casting and that barely any Sn can be detected adjacent to the Al_2Cu grains growing at the surface. Instead, Sn are observed distributing in the eutectic Al_2Cu–Al structure. Interestingly, as seen through the EDS analysis, Mg is also detected in several of these Sn-rich areas.

A further phase identification of the intermetallic particles forming at the aluminum/copper interface was conducted using EBSD. Fig. 11a–c shows the image quality map, orientation map and phase map, respectively. In the image quality map, the contrast shows that copper can be found at the top whereas aluminum is seen in the bottom of the image in between the Al_2Cu phase. Due to their similar crystal structure, the Al and Cu could not be separated in the phase map and both are thus shown in green in Fig. 11c. By comparing the orientation map and phase map, it can be seen that the Al_2Cu phase has quite large grains, whereas the thin intermetallic layer at the surface of the copper is predominated with small Al_4Cu_9 particles. In between the Al_4Cu_9 grains

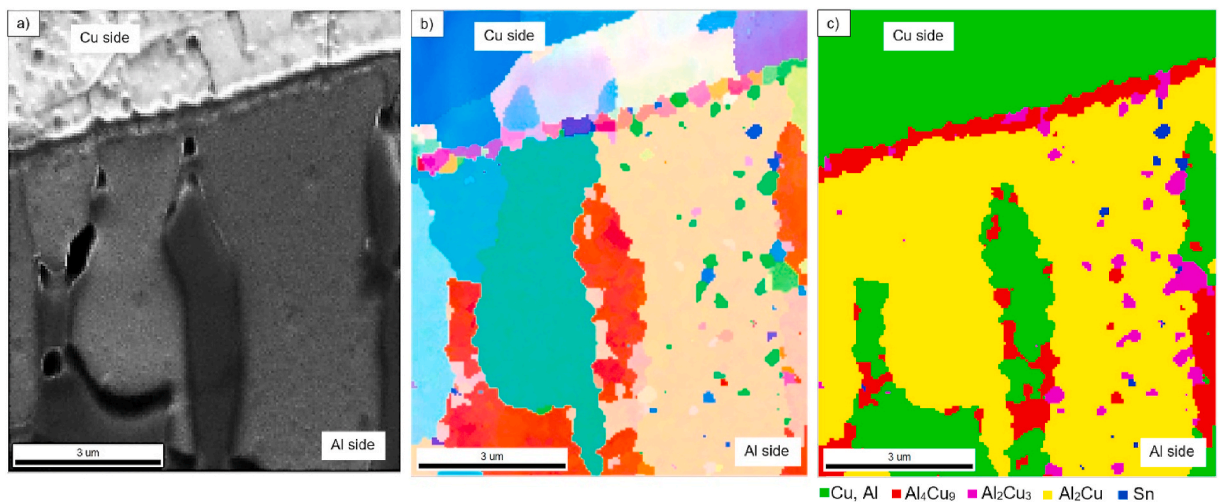

Fig. 11. EBSD results from the A356/Cu interface in a casting with Sn-coating. a) Image quality map, b) Orientation map and c) Phase map.

and the coarse Al_2Cu particles, some Al_2Cu_3 grains can also be detected. However, only few Sn particles can be detected along the coarse Al_2Cu particles, which is consistent with the previous element mapping results.

3.3. Tensile strength of the metallurgical bond

During the tensile testing, brittle fracture occurred in all samples and therefore tensile strength and ultimate tensile strength (UTS) had the same value. From all the samples, an average UTS of 55.8 MPa with a standard deviation of 27.5 MPa was measured, whereas the maximum UTS measured was 90.8 MPa. The difference in average and maximum UTS was attributed to variations in the shape and thickness of the binary Al–Cu phases in the reaction layer adjacent to the copper surface. Fig. 12 shows the stress-strain curve for the tensile sample where a maximum UTS was achieved. From the figure it can be seen that fracture occurs at approximately 0.16% strain, showing clear brittle fracture.

Fig. 13a–c shows the A356/Cu interface after tensile testing as well as the fracture surfaces in a tensile sample with minimum UTS, while similar images for a fractured tensile sample with maximum UTS are shown in Fig. 13d–f. In the BSE image of the tensile sample with minimum UTS, Fig. 13a, a crack can be seen propagating through the coarse and continuous Al–Cu intermetallic layer at the copper surface on the left side, which implies that the thick Al–Cu intermetallic layer is the weakest part in terms of strength. This can also be observed on the fracture side, where the majority of the interfacial intermetallic layer has been broken off from the bulk copper side, while the Al–Cu intermetallic phases can only be observed in some very small local areas. From the fracture surfaces in Fig. 13b and c, Al_2Cu is the dominating phase detected. In addition, Cu-rich phases such as AlCu, Al_3Cu_4 and Al_4Cu_9 can be found, confirming that the fracture has propagated through the Al–Cu intermetallic layer at the Cu surface. Fig. 13d shows a BSE image of the interface of the fractured tensile sample with maximum UTS. As can be seen, the interfacial intermetallic layer in this sample is thinner and more uniform compared to that in Fig. 13a, and no cracks exist in the interfacial layer. From the fractured side of the interface (right side), it can be seen that most of the Al–Cu intermetallic phases are left on the copper side after fracture, where the fracture has propagated through the coarse Al–Al_2Cu eutectic layer. The fracture surfaces in Fig. 13d and f show a brittle fracture character of the tensile sample. However, both stripes and grooves can be observed. On the fracture surface of the Cu side, no Cu phase can be detected. Instead, it is covered by eutectic Al–Al_2Cu and intermetallic phases of Al_2Cu, AlCu and Al_2Cu_3. This confirms that the fracture has occurred in the intermetallic

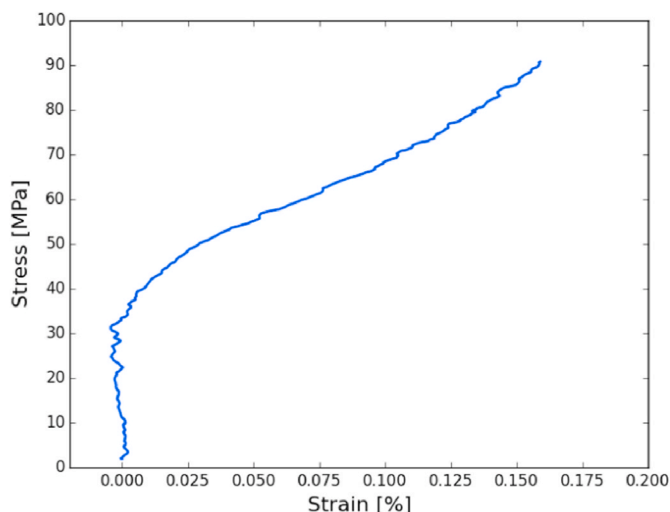

Fig. 12. Stress-strain curve of the Al/Cu tensile sample where the highest tensile strength of 90.8 MPa was achieved.

bonding layer. It is interesting to see that the majority of the fracture surface area shows parallel stripes and grooves, which is corresponding to the coarse eutectic Al_2Cu particles, separated by a thin eutectic Al phase, growing directly from the Al_4Cu_9 and Al_2Cu_3 intermetallic layer. A small fraction of the fracture area consists of an Al–Al_2Cu structure, which is supposed to be Al–Al_2Cu eutectics that form freely in the interfacial region. Also, a small fraction of the fracture surface shows a very smooth appearance, consisting of pure AlCu and Al_2Cu_3, showing that the fracture has been locally propagating through the pure intermetallic layer.

4. Discussion

In the phase diagram of Al–Cu alloys, there is a eutectic point at 548°C at which copper has a solubility of 5.65 wt% in aluminum [27]. Therefore, it is expected that a reaction between the two metals will occur at temperatures above the eutectic temperature. However, the results in Fig. 7a show that reactions only occurred in a few local areas in the uncoated compound casting. This is consistent with the wetting test, where the reaction between the A356 droplet and copper substrate only occurred after a long holding time at 750°C. Zare, Divandari and Arabi reported that when the surface oxide layers naturally present on both the solid Cu and liquid A356 surfaces are trapped between the two, insufficient wetting and no metallurgical bonding were obtained [28]. Similarly, in the present research, without surface coating the oxide layer on both the copper and aluminum melt surfaces will prevent complete wetting between the two metals. However, when a Sn-coating is applied to the copper, complete wetting can be achieved, and continuous metallurgical bonding was obtained in the castings. The coating layer prior to casting was found to consist of pure Sn, as well as Cu_6Sn_5 and Cu_3Sn. This appearance coincides with that reported in soldering processes, where Cu_6Sn_5 is the first phase to form, followed by Cu_3Sn which in the end grows at the expense of Cu_6Sn_5 [29]. However, the intermetallic phases in the Cu–Sn system are considered brittle, especially Cu_6Sn_5 as it grows into large scallop-shaped grains [30,31]. In the wetting experiment, interdiffusion of Sn and Cu occurs during heating. Sn has a low melting point of 232°C [22] and low solubility in aluminum, with no intermetallic phases present in the binary Al–Sn alloys [32]. When reaching the holding temperature of 750°C during the wetting experiment, the Sn-layer has completely melted. However, the binary Cu–Sn phases were not detected in neither the droplet/substrate interface nor the casting interface after solidification, showing that the Cu–Sn intermetallic phases in the coating layer could completely dissolve in the Al melt. In a wetting experiment between liquid Sn and Al, Lin et al. achieved good wetting at 400°C, with a final contact angle of approximately 30°, which was ascribed to the penetration of the liquid Sn into cracks in the aluminum oxide layer that formed due to differences in thermal expansion coefficients of the different materials [33]. It has also been reported that formation of intermetallic phases improve wettability as the phases can replace the oxidized surface [34]. Here, it seems that the Sn melt on the Cu substrate could penetrate and break up the oxide layer covering the aluminum melt. The high affinity between aluminum and copper at elevated temperatures [11] can cause the formation of intermetallic phases and complete wetting between the metals. Similarly, in the casting experiment, the Sn-layer will melt and contribute to break up the surface oxide layer of the aluminum melt, not only through liquid penetration, but also likely through mechanical abrading from liquid flow. Thus, the aluminum and copper are free to react without the hindrance of an oxide layer.

With the significantly improved wettability between the A356 aluminum melt and the Sn-coated copper, the Cu insert in the compound castings can react sufficiently with the Al melt. As a result, a relatively thick reaction area has formed between the two metals. However, considering the tensile strengths measured, the average value of 55.8 MPa is significantly higher compared to that reported for compound castings between aluminum and Zn-coated copper of 26 MPa [3]. The

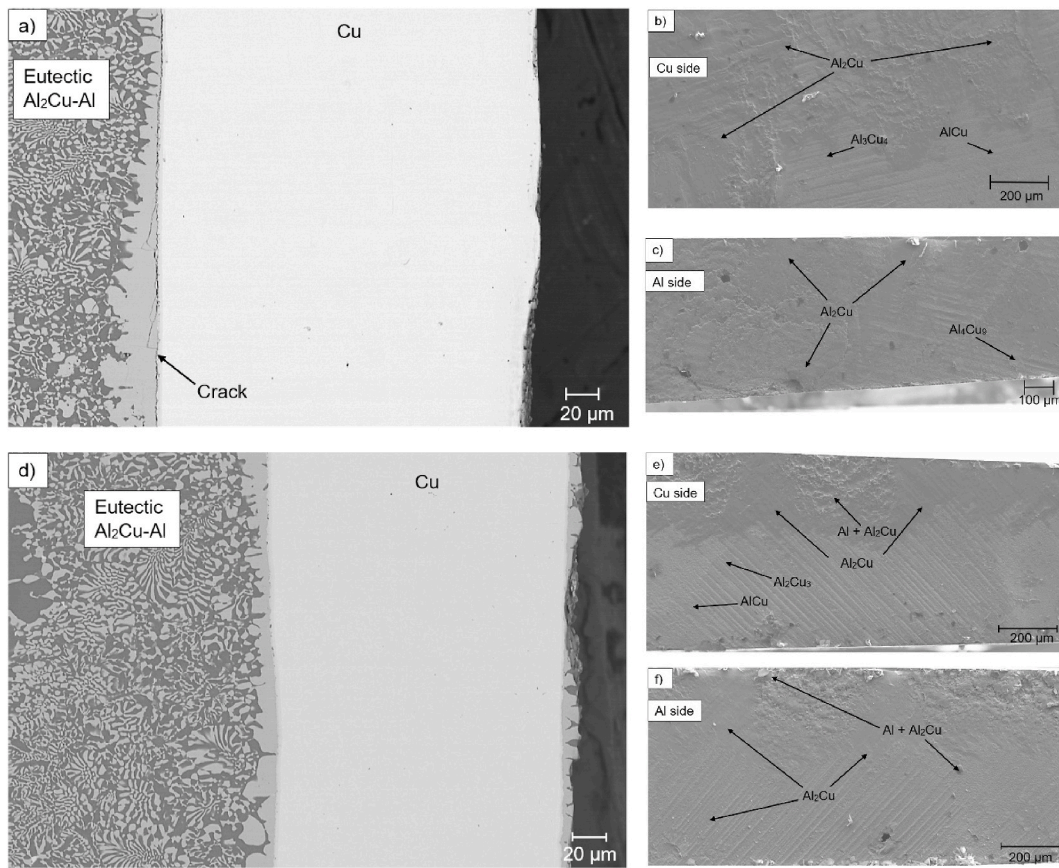

Fig. 13. Interfacial microstructure after tensile testing in a) a sample with minimum UTS, with fracture surfaces in b) Cu side and c) Al side, and d) a sample with maximum UTS, with fracture surfaces in e) Cu side and f) Al side.

maximum tensile strength of 90.8 MPa is close to that of 105.8 MPa obtained for friction stir welded 6061/Cu [16]. What should be noted, is that the thickness of the reaction layer in most casting samples were close to 1 mm. Previous studies have reported that strength of the Al/Cu interface decreases with increasing reaction layer thickness, especially the copper-rich phases [3,35], which is a reason why welded Al/Cu joints previously have shown much higher bonding strength compared to cast Al/Cu joints [17]. However, the results obtained in this research shows that it is possible to obtain similar bonding strength to that of welded Al/Cu components with thinner reaction layers. Also, it can thus be expected that the strength of the Al/Cu compound casting aided by Sn-coating can be further improved by reducing the reaction layer thickness. This can be achieved by increasing the solidification rate during compound casting to reduce the reaction time between the Al melt and Cu inserts. As Sn has a low melting point, re-melting of the coating layer can occur with little to no preheating of the mold and insert, which then would result in a thinner reaction layer. Additionally, it should be further investigated if a thinner Sn coating layer can affect thickness of the reaction layer.

By comparing the microstructure of the compound castings with and without Sn-coating, some differences can be observed. Without Sn-coating, Q-phase ($Al_5Cu_2Mg_8Si_6$) formed adjacent to the eutectic Al_2Cu. In the Sn-coated compound castings however, the Q-phase was not detected. Instead, high Mg concentrations were found in the Sn-rich areas, suggesting that some Sn–Mg rich particles may have formed. The formation of such particles can consume a lot of Mg in the Al melt, reducing the chance of Q-phase forming. Compared to the castings without Sn-coating, the fraction of the primary Si particles was much lower, while the particles were much finer. Previous compound casting experiments between A356 and Cu have also shown formation of large primary Si particles [21,36]. These were believed to form as a result of high cooling rate at the Cu surface. In a previous study by the present authors, it was suggested that the primary Si particles formed due to the reaction between phosphorous present in the Cu pipes as an impurity element and aluminum forming AlP [26]. The AlP particle can act as nucleation sites for silicon. In the present research, phosphorus-deoxidized copper, with a concentration of 0.015–0.040 wt % P was used. Ho and Cantor reported that a concentration of 0.25–2 ppm P in the Al melt is sufficient to precipitate AlP particles and nucleate Si particles at a low undercooling [37]. Thus, the phosphorous present in the copper pipes would be sufficient to form AlP when parts of the Cu insert dissolves in the liquid A356. As primary silicon particles can be observed throughout the relatively thick reaction areas, the cooling effect of the copper insert will not be as significant. Thus, the results obtained in this work seems to agree with the AlP theory. The finer distribution of Si particles in the Sn-coated compound castings can then be attributed to the larger reaction areas, causing a full diffusion of P atoms in the copper insert into the Al melt and therefore a lower concentration of P. This refinement is also believed to improve the bonding strength of the compound casting, as Si particles are known to be brittle and refinement of large eutectic Si particles is commonly used to improve strength and ductility of hypereutectic Al–Si alloys [38,39].

5. Conclusions

In this work, a novel coating method of hot dip Sn-coating has been applied to copper inserts prior to compound casting with aluminum A356. The effects of the coating layer on the aluminum/copper interfacial microstructure and bonding strength have been discussed. In addition, sessile drop tests were conducted to study the influence of the Sn coating layer on the wettability between Al melt and Cu. From the results presented, the following conclusions can be made:

The wettability between A356 aluminum melt and solid Cu is significantly improved with the application of a Sn-coating to the Cu substrate. Sessile drop wetting tests at 750°C show that a complete wetting can be achieved between Al melt and the Sn-coated Cu substrate, whereas without coating only local reaction regions show good wetting.

Successful compound casting has been achieved between Sn-coated copper inserts and A356 aluminum alloy, where crack-free continuous metallurgical bonding forms at the interface. The Sn coating layer was completely melted, and fine Sn-rich particles were observed adjacent to the eutectic Al_2Cu phase in the final interfacial microstructure.

Al–Cu phases are the main intermetallic phases observed in the reaction layer. From the surface of the Cu insert towards the cast A356 alloy, thin layers of Al_4Cu_9 and Al_2Cu_3, coarse Al_2Cu particles and a fine Al–Al_2Cu eutectic structure are observed.

Primary silicon particles were more finely distributed and of smaller size in the reaction area of the Sn-coated compound castings. This was ascribed to the thick reaction layer at the interface, which reduce the P concentration in the melt.

An average tensile strength of 55.8 MPa and a maximum tensile strength of 90.8 MPA were obtained in the Sn-coated compound castings. The brittle fracture mainly occurs through the coarse Al_2Cu and the Al–Al_2Cu eutectic region.

CRediT authorship contribution statement

Aina Opsal Bakke: Methodology, Validation, Investigation, Writing – original draft, Visualization. **Lars Arnberg:** Supervision, Writing – review & editing, Visualization. **Yanjun Li:** Methodology, Supervision, Writing – review & editing, Visualization.

Declaration of competing interest

The authors declare that they have no known competing financial interests or personal relationships that could have appeared to influence the work reported in this paper.

Acknowledgements

The authors are grateful for the Research Council of Norway for financial support through the IPN project AluLean (project number 90141902), Aludyne Norway AS for contribution of materials and SINTEF for facilities and help with the wetting experiments.

References

[1] L.Y. Sheng, F. Yang, T.F. Xi, C. Lai, H.Q. Ye, Influence of heat treatment on interface of Cu/Al bimetal composite fabricated by cold rolling, Compos. B Eng. 42 (6) (2011) 1468–1473, https://doi.org/10.1016/j.compositesb.2011.04.045.
[2] W.E. Veerkamp, Copper-to-Aluminum transitions in high direct-current bus systems, Proceedings of Industry Applications Society 42nd Annual Petroleum and Chemical Industry Conference (1995) 187–194, https://doi.org/10.1109/PCICON.1995.523953.
[3] T. Liu, Q. Wang, Y. Sui, Q. Wang, D. Wenjiang, An investigation into interface formation and mechanical properties of aluminum-copper bimetal by squeeze casting, Mater. Des. 89 (2016) 1137–1146, https://doi.org/10.1016/j.matdes.2015.10.072.
[4] N. Ahmed, Extrusion of copper clad aluminum wire, J. Mech. Work. Technol. 2 (1978) 19–32, https://doi.org/10.1016/0378-3804(78)90012-8.
[5] W.-B. Lee, K.-S. Bang, S.-B. Jung, Effects of intermetallic compound on the electrical and mechanical properties of friction welded Cu/Al bimetallic joints during annealing, J. Alloys Compd. 390 (1–2) (2005) 212–219, https://doi.org/10.1016/j.jallcom.2004.07.057.
[6] C.W. Tan, Z.G. Jiang, L.Q. Li, Y.B. Chen, X.Y. Chen, Microstructural evolution and mechanical properties of dissimilar Al–Cu joints produced by friction stir welding, Mater. Des. 51 (2013) 466–473, https://doi.org/10.1016/j.matdes.2013.04.056.
[7] M. Abbasi, A.K. Taheri, M.T. Salehi, Growth rate of intermetallic compounds in Al/Cu bimetal produced by cold roll welding process, J. Alloys Compd. 319 (1–2) (2001) 233–241, https://doi.org/10.1016/S0925-8388(01)00872-6.
[8] A. Khosravifard, R. Ebrahimi, Investigation of parameters affecting interface strength in Al/Cu clad bimetal rod extrusion process, Mater. Des. 31 (2010) 493–499, https://doi.org/10.1016/j.matdes.2009.06.026.
[9] G. Liu, X. Hu, Y. Fu, Y. Li, Microstructure and mechanical properties of ultrasonic welded joint of 1060 aluminum alloy and T2 pure copper, Met 7 (9) (2017), https://doi.org/10.3390/met7090361.
[10] M. Braunovic, N. Aleksandrov, Effect of electrical current on the morphology and kinetics of formation of intermetallic phases in bimetallic aluminum-copper joints, Proceedings of IEEE Holm Conference on Electrical Contacts (1993) 261–268, https://doi.org/10.1109/HOLM.1993.489685.
[11] M.S. Mohebbi, A. Akbarzadeh, Fabrication of copper/aluminum composite tubes by spin-bonding process: experiments and modeling, Int. J. Adv. Manuf. Technol. 54 (9–12) (2011) 1043–1055, https://doi.org/10.1007/s00170-010-3016-5.
[12] X.-G. Wang, X.-G. Li, F.-J. Yan, C.-G. Wang, Effect of heat treatment on the interfacial microstructure and properties of Cu-Al joints, Weld. World 61 (1) (2017) 187–196, https://doi.org/10.1007/s40194-016-0393-x.
[13] L. Pan, P. Li, X. Hao, J. Zhou, H. Dong, Inhomogeneity of microstructure and mechanical properties in radial direction of aluminum/copper friction welded joints, J. Mater. Process. Technol. 255 (2018) 308–318, https://doi.org/10.1016/j.jmatprotec.2017.12.027.
[14] M. Asemabadi, M. Sedighi, M. Honarpisheh, Investigation of cold rolling influence on the mechanical properties of explosive-welded Al/Cu bimetal, Mater. Sci. Eng. A 558 (2012) 144–149, https://doi.org/10.1016/j.msea.2012.07.102.
[15] N. Sharma, Z.A. Khan, A.N. Siddiquee, Friction stir welding of aluminum to copper—an overview, Trans. Nonferrous Metals Soc. China 27 (10) (2017) 2113–2136, https://doi.org/10.1016/S1003-6326(17)60238-3.
[16] K.P. Mehta, V.J. Badheka, Effects of tilt angle on the properties of dissimilar friction stir welding copper to aluminum, Mater. Manuf. Process. 31 (3) (2016) 255–263, https://doi.org/10.1080/10426914.2014.994754.
[17] A.O. Al-Roubaiy, S.M. Nabat, A.D.L. Batako, Experimental and theoretical analysis of friction stir welding of Al–Cu joints, Int. J. Adv. Manuf. Technol. 71 (9) (2014) 1631–1642, https://doi.org/10.1007/s00170-013-5563-z.
[18] R.K. Tayal, V. Singh, S. Kumar, R. Garg, Compound casting - a literature review, in: Proceedings of the National Conference on Trends and Advances in Mechanical Engineering, 2012, pp. 501–510.
[19] Y. Hu, Y.-q. Chen, L. Li, H.-d. Hu, Z.-a. Zhu, Microstructure and properties of Al/Cu bimetal in liquid–solid compound casting process, Trans. Nonferrous Metals Soc. China 26 (6) (2016) 1555–1563, https://doi.org/10.1016/S1003-6326(16)64261-9.
[20] M. Pintore, J. Wölck, T. Mittler, T. Greß, W. Volk, Composite casting and characterization of Cu-Al bilayer compounds, Inter. Metalcast. 14 (1) (2020) 155–166, https://doi.org/10.1007/s40962-019-00344-x.
[21] W. Jiang, F. Guan, G. Li, H. Jiang, J. Zhu, Z. Fan, Processing of Al/Cu bimetal via a novel compound casting method, Mater, Manuf. Process. 34 (9) (2019) 1016–1025, https://doi.org/10.1080/10426914.2019.1615084.
[22] G. Aylward, T. Findlay, SI Chemical Data, fifth ed., John Wiley & Sons Australia, Milton, 2002.
[23] K.J.M. Papis, J.F. Löffler, P.J. Uggowitzer, Interface formation between liquid and solid Mg alloys-An approach to continuously metallurgic joining of magnesium parts, Mater. Sci. Eng. A 527 (9) (2010) 2274–2279, https://doi.org/10.1016/j.msea.2009.11.066.
[24] W. Jiang, Z. Fan, G. Li, C. Li, Effects of zinc coating on interfacial microstructures and mechanical properties of aluminum/steel bimetallic composites, J. Alloys Compd. 678 (2016) 249–257, https://doi.org/10.1016/j.jallcom.2016.03.276.
[25] J.-l. Zhao, J.-c. Jie, F. Chen, H. Chen, T.-j. Li, Z.-q. Cao, Effect of immersion Ni plating on interface microstructure and mechanical properties of Al/Cu bimetal, Trans. Nonferrous Metals Soc. China 24 (2014) 1659–1665, https://doi.org/10.1016/S1003-6326(14)63238-6.
[26] A.O. Bakke, J.-O. Løland, S. Jørgensen, J. Kvinge, L. Arnberg, Y. Li, Interfacial microstructure formation in Al7SiMg/Cu compound castings, Inter. Metalcast. 15 (2021) 40–48, https://doi.org/10.1007/s40962-020-00463-w.
[27] T.B. Massalski, The Al−Cu (Aluminum-Copper) system, Bull. Alloy Phase Diagr. 1 (1) (1980) 27–33, https://doi.org/10.1007/BF02883281.
[28] G.R. Zare, M. Divandari, H. Arabi, Investigation on interface of Al/Cu couples in compound casting, Mater. Sci. Technol. 29 (2) (2013) 190–196, https://doi.org/10.1179/1743284712Y.0000000096.
[29] J.F. Li, P.A. Agyakwa, C.M. Johnson, Interfacial reaction in Cu/Sn/Cu system during the transient liquid phase soldering process, Acta Mater. 59 (3) (2011) 1198–1211, https://doi.org/10.1016/j.actamat.2010.10.053.
[30] M. Zhao, L. Zhang, Z.-Q. Liu, M.-Y. Xiong, L. Sun, Structure and properties of Sn-Cu lead-free solders in electronics packaging, Sci. Technol. Adv. Mater. 20 (1) (2019) 421–444, https://doi.org/10.1080/14686996.2019.1591168.
[31] M.S. Park, S.L. Gibbons, R. Arróyave, Phase-field simulations of intermetallic compound growth in Cu/Sn/Cu sandwich structure under transient liquid phase bonding conditions, Acta Mater. 60 (18) (2012) 6278–6287, https://doi.org/10.1016/j.actamat.2012.07.063.
[32] T.B. Massalski, H. Okamoto, P.R. Subramanian, L. Kacprzak, Binary Alloy Phase Diagrams, second ed., ASM International, Materials Park, Ohio, USA, 1990.
[33] Q. Lin, W. Zhong, F. Li, W. Yu, Reactive wetting of tin/steel and tin/aluminum at 350–450 °C, J. Alloy, Compd 716 (2017) 73–80, https://doi.org/10.1016/j.jallcom.2017.05.036.
[34] P. Protsenko, A. Terlain, V. Traskine, N. Eustathopoulos, The role of intermetallics in wetting in metallic systems, Scripta Mater. 45 (12) (2001) 1439–1445, https://doi.org/10.1016/S1359-6462(01)01181-2.
[35] S. Tavassoli, M. Abbasi, R. Tahavvori, Controlling of IMCs layers formation sequence, bond strength and electrical resistance in Al-Cu bimetal compound casting process, Mater. Des. 108 (2016) 343–353, https://doi.org/10.1016/j.matdes.2016.06.076.

[36] M. Divandari, A.R.V. Golpayegani, Study of Al/Cu rich phases formed in A356 alloy by inserting Cu wire in pattern in LFC process, Mater. Des. 30 (8) (2009) 3279–3285, https://doi.org/10.1016/j.matdes.2009.01.008.
[37] C.R. Ho, B. Cantor, Heterogeneous nucleation of solidification of Si in Al-Si and Al-Si-P alloys, Acta Metall. Mater. 43 (8) (1995) 3231–3246, https://doi.org/10.1016/0956-7151(94)00480-6.
[38] A. Knuutinen, K. Nogita, S.D. McDonald, A.K. Dahle, Modification of Al–Si alloys with Ba, Ca, Y and Yb, J. Light Met. 1 (4) (2001) 229–240, https://doi.org/10.1016/S1471-5317(02)00004-4.
[39] J. Rao, J. Zhang, R. Liu, J. Zheng, D. Yin, Modification of eutectic Si and the microstructure in an Al-7Si alloy with barium addition, Mater. Sci. Eng. A 728 (2018) 72–79, https://doi.org/10.1016/j.msea.2018.05.010.